Heliyon 7 (2021) e06657

Contents lists available at ScienceDirect

Heliyon

journal homepage: www.cell.com/heliyon

Research article

Design and identification of novel annomontine analogues against SARS-CoV-2: An *in-silico* approach

Kamran Waidha [a], Anjali Saxena [a], Prashant Kumar [a], Sunil Sharma [b], Devalina Ray [a], Biswajit Saha [a,*]

[a] Amity Institute of Biotechnology, Amity University Uttar Pradesh, Noida, 125, 201301, India
[b] Chemical Engineering Department, National Tsing Hua University, Hsinchu 30013, Taiwan

ARTICLE INFO

Keywords:
COVID-19
Molecular docking
ADME/Tox
SARS-CoV-2
Annomontine
β- carboline

ABSTRACT

Aims: COVID-19 has currently emerged as the major global pandemic affecting the lives of people across the globe. It broke out from Wuhan Province of China, first reported to WHO on 31st December 2019 as "Pneumonia of unknown cause". Over time more people were infected with this virus, and the only tactic to ensure safety was to take precautionary measures due to the lack of any effective treatment or vaccines. As a result of unavailability of desired efficacy for previously repurposed drugs, exploring novel scaffolds against the virus has become the need of the hour.

Main methods: In the present study, 23 new annomontine analogues were designed representing *β*-Carboline based scaffolds. A hypothesis on its role as an effective ligand was laid for target-specific binding in SARS-CoV-2. These molecules were used for molecular docking analysis against the multiple possible drug targets using the Maestro Interface. To ensure the drug safety of these molecules ADME/Tox analysis was also performed.

Key findings: The molecular docking analysis of the 23 novel molecules indicated the efficiency of these derivates against COVID-19. The efficiency of molecules was computed by the summation of the docking score against each target defined as $Lig_{E\ Score}$ and compared against Hydroxycholoquine as a standard. Based on the docking score, the majority of the annomontine derivatives were found to have increased binding affinity with targets as compared to hydroxycholoquine.

Significance: Due to the lack of efficiency, effectiveness, and failure of already repurposed drugs against the COVID-19, the exploration of the novel scaffold that can act as effective treatment is much needed. The current study hence emphasizes the potential of Annomontine based - *β*- Carboline derivatives as a potential drug candidate against COVID-19.

1. Introduction

COVID-19 pandemic broke out from Wuhan Province of China, first reported to WHO on 31st December 2019 as "Pneumonia of unknown cause". As of 16th August 2020, there were confirmed 21,260,760 infective cases and 761,018 death cases globally (Table 1). In India, according to situation update report-27, updated on 2nd August 2020, there are 1,695,988 confirmed cases and 36,511 deaths in around 32 states/UTs with numbers increasing at an exponential rate both in India and at global level. Severe acute respiratory syndrome-coronavirus 2 also referred to as SARS-COV-2, which is a 26.7 kb–31.7 kb positive-sense RNA virus covered with an envelope, causes COVID-19. It is spherical or pleomorphic in shape bearing projection of glycoprotein on its surface [1].

The symptoms of COVID-19, which appear post-incubation period of approximately 5.2 days include common symptoms such as cough, fever, fatigue, and soar throat while other symptoms are diarrhea, dysphonia, headache, coughing up blood, low level of lymphocytes and production of sputum [2, 3, 4, 5, 6]. The pathogenesis of COVID–19 infection is severe pneumonia, RNAaemia with co-occurrences of acute cardiac injury and GGO (ground-glass opacities). Patients infected with COVID-19 show significantly increased blood levels of chemokine and cytokine such as IL7, IL8, TNF-alpha, VEGFA, and others. In severe cases, increased levels of pro-inflammatory cytokines such as IL2, IL10, and others can be found in blood reasoned for its severe progression [3].

SARS – CoV-2 belongs to *β*-CoV genera, showing 88% similarity with bat-SL-CoVZC45 and bat-SL-CoVZXC21 and 50% similarity with

* Corresponding author.
E-mail address: biswasaha@gmail.com (B. Saha).

https://doi.org/10.1016/j.heliyon.2021.e06657
Received 8 July 2020; Received in revised form 20 August 2020; Accepted 29 March 2021

Table 1. Number of cases of COVID-19 world-wide till 3rd August 2020.

S. No	Region/Territory	Number of Cases	
		Diagnosed (Confirmed)	Death
1.	Globally	17918582	686703
2.	Western Pacific Region	327617	8450
3.	European Region	3391779	213559
4.	South-East Asia Region	2187015	46675
5.	Eastern Mediterranean Region	1564836	40782
6.	Region of the Americas	9630598	363162
7.	African Regions	815996	14062

MERS-CoV sequence [7]. The genome consists of about 10 ORFs, ORF1a and ORF1b which contribute to approximately 75% of its viral RNA are translated into two viral replicase polyproteins PP1a and PP1b [8]. PP1a/b are further processed into sixteen non-structural proteins forming viral replicase transcription complex [8, 9]. The remaining 25% genome composed of other ORFs encode the structural proteins i.e. spike (S), envelop (E), membrane (M), nucleocapsid (N), and other accessory proteins which do not play any role in its viral replication [8, 9]. Various studies have reported the entry of the COVID-19 virus into the host cell through the interaction of spike (S) glycoprotein binding with angiotensin-converting enzyme 2 (ACE 2) [10]. After entry of virus RNA genome into the host cell cytoplasm, it is translated into PP1a/b and structural proteins initiating the process of viral replication, envelop glycoproteins are inserted in the membrane of either golgi bodies or endoplasmic reticulum. The nucleocapsid formation takes place by the combination of genomic RNA and nucleocapsid RNA, after which the viral particles replicate in an intermediate compartment between the endoplasmic reticulum and golgi known as ERGIC. Finally, these viral particle fuses with the plasma membrane to release the virus [11, 12].

Currently, SARS-CoV-2 has no specific clinically proven antiviral agent to protect against its infection just like SARS-CoV and MERS -CoV [12, 13]. However, several potential therapeutic targets are available for either repurposing of already existing antiviral drugs or to develop novel and effective intervention methods.

A recent report has identified 332 high confidence SARS-CoV-2 – Human Protein-Protein interaction (PPI) among those, 66 are identified as druggable human protein or host factors [14]. Various existing drugs (Figure 1) are under trial for protection against SARS-CoV-2, among them remdesivir, which is administrated intravenously was expected to possess significant potential. Similarly, a couple of other drugs such as chloroquine and hydroxychloroquine (HCQ) in combination with azithromycin are under investigation [15, 16].

However, both hydroxychloroquine and remdesivir performed poorly in trials against COVID-19, therefore, further uprising the demand for new drugs and vaccines. In this study, we have designed novel natural product alkaloid based annomontine derivatives, which have been known for various biological activities over decades. In continuation to our ongoing research on the design and synthesis of bioactive molecules related to β-carboline derivatives, diversely functionalized annomontines are developed based on Figure 2 [17,18].

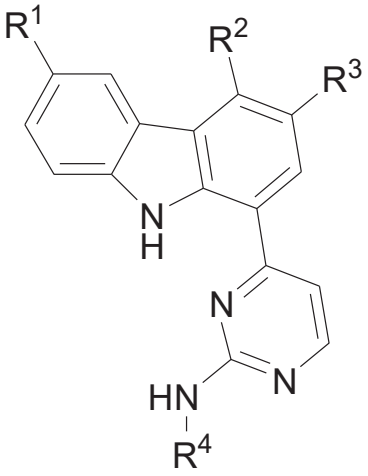

Figure 2. Annomontine skeleton.

Annomontine is a class of heterocyclic alkaloids extracted from the trunk and root bark of certain plants belonging to the *Annonaceae* family and structurally represented by pyrimidine substituted β-carbolines [19, 20]. The β-carboline alkaloids in turn can be categorized as an indole alkaloid that contains a mutual tricyclic pyrido indole ring structure. β-carbolines can be further subdivided and identified according to the degree of saturation in the *N*-containing fused six-membered ring. Complete unsaturation in the six-membered heterocyclic ring leads to fully aromatic β-carbolines (βCs), whereas the partial or complete saturation in the same ring generates dihydro-β-carbolines (βDHCs) and tetrahydro-β-carbolines (THβCs), respectively [21, 22]. In general, β-carboline alkaloid exhibits a wide range of pharmacological activities in addition to antiparasitic, particularly against *Leishmania* sp., *Plasmodium falciparum,* and *Trypanosoma cruzi.* Furthermore, harmaline and harmine which are also derived from β-carboline alkaloid show anxiolytic activity in the elevated pulse and maze [23, 24]. In the vast category of naturally occurring βCs, the pyrimidine-β-carboline alkaloids are the rarest class of compounds that has only three existing members, structurally interpreted by a 2-aminopyrimidine unit linked to a harman moiety and interesting from both structural and biological points of view. In

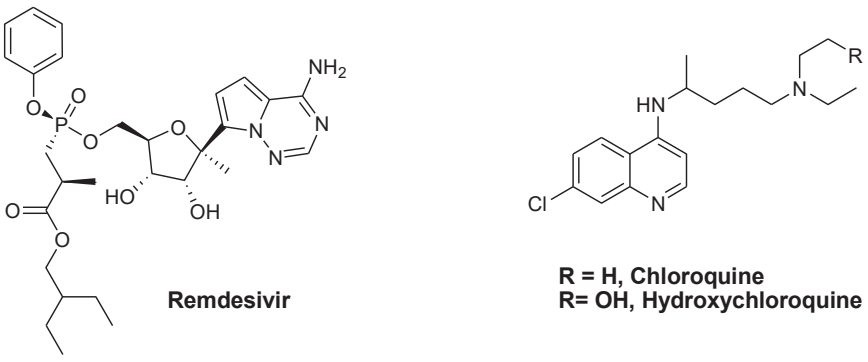

Figure 1. Structures of existing drug molecules under trial for protection against SARS-CoV-2.

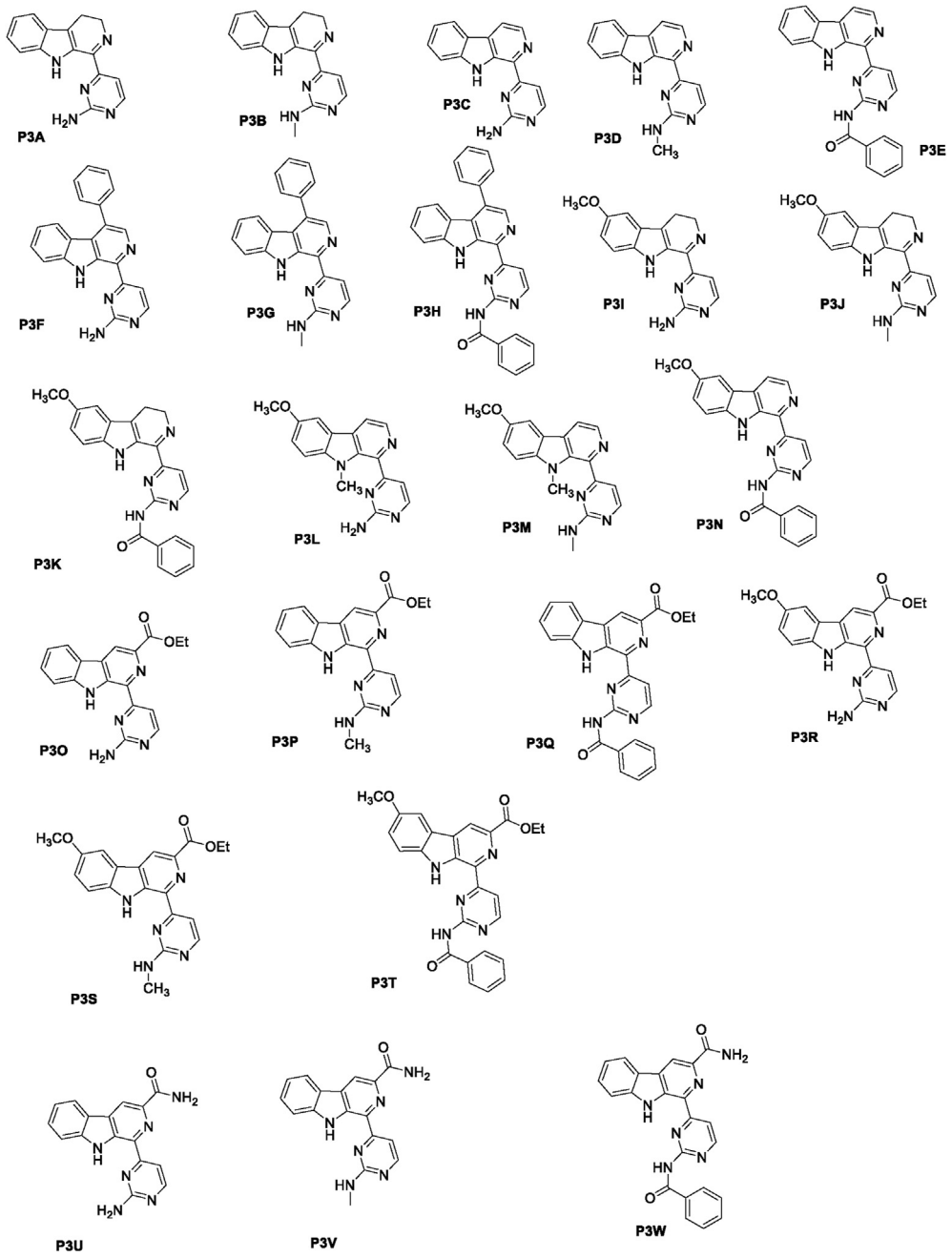

Figure 3. Structure of Annomontine based derivatives.

Table 2. List of PDB Protein Structures used in the study.

Protein	PDB ID	Resolution (Angstrom)
M^{PRO}	6Y2F	1.95 Å
PL^{PRO}	6W9C	2.7Å
ACE2	6M0J	2.45Å
Spike Protein	6M0J	2.45Å
NSP 9	6W4B	2.95Å
TMPRSS2	Homology Modelled	

Table 3. Grid Size and Grid center Coordinates used for molecular docking.

Protein	Size	Grid Coordinates		
	(x,y,z) Angstrom	X	Y	Z
M^{Pro}	20,20,20	10.9166	-0.50212	20.81104
ACE 2	20,20,20	-24.7760	35.20782	-17.43447
Spike Protein	20,20,20	-38.6562	43.2729	12.51189
NSP 9	20,20,20	57.79818	-0.7736	21.9645
PL^{Pro}	20,20,20	-44.6608	35.2642	12.4375

general, the β-carboline analogs have been synthesized enormously and widely explored for bioactivity. However, to date, limited report exists on the synthesis of annomontine derivatives which represents a special class of β-carboline [25, 26].

We have designed 23 novel annomontine analogs (Figure 3) and docked them against the various molecular targets for SARS-CoV-2 and humans such as M^{PRO}, PL^{PRO}, spike protein, ACE2, and TMPRSS2 respectively to validate them as potential molecules for future investigation against SARS-Cov-2.

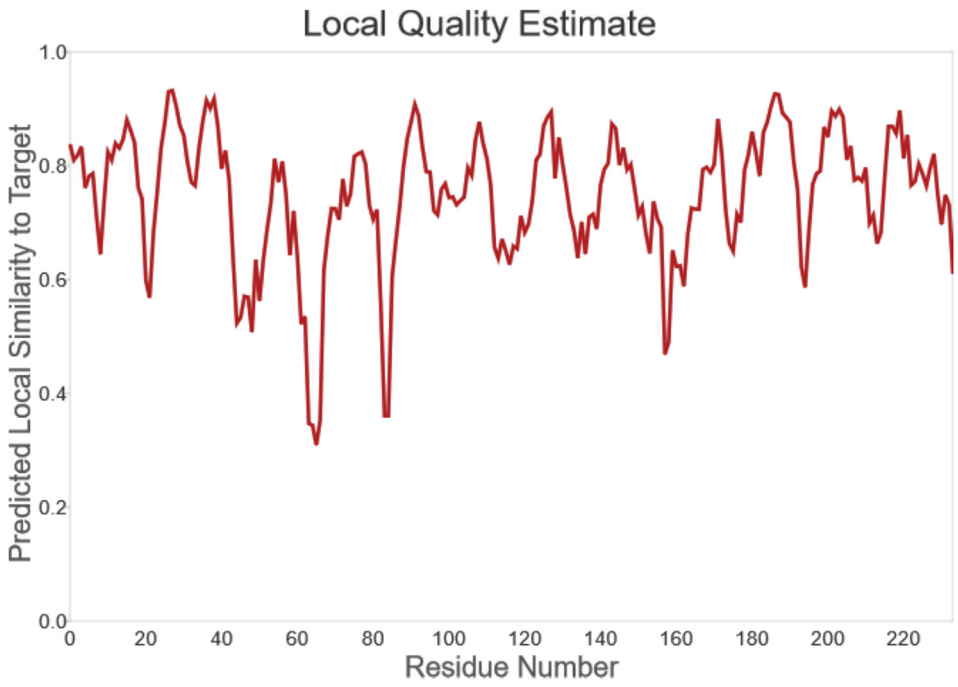

Figure 4. Structure validation of modelled TMPRSS2: (A) Local quality estimate of the residues of the predicted TMPRSS2 model 1.

2. Material and methods

2.1. Ligand design and preparation

The ligand structures of annomontine derivatives were designed using ChemDraw (Figure 3). The 3D structure generation, preparation, and geometry optimization with energy minimization of a total of 23 ligands were executed using the LigPrep module of Schrodinger suite. All the ligands were prepared by adding hydrogen atoms, salt removing, and ionizing at physiological pH 7 (±2). OPLS3e force field was employed for energy minimization and RMSD cut-off 0.01 Å was selected to generate low energy state isomers.

2.2. Protein structure retrieval

3D structures of target proteins for COVID-19 were retrieved using protein data bank. The list of structures retrieved are given in Table 2 along with their respective PDB IDs. The protein structures were short-listed based on the literature review.

2.3. Homology Modelling and structure validation of TMPRSS2

TMPSS2 is one of the upcoming potential targets considered for SARS-CoV-2. The catalytic domain of protein was homology modelled using expasy Swiss-Model [27]. Two models were constructed using different templates with a sequence identity of 44.87% and 42.92% respectively. The structure assessment was executed using MolProbity and Verify3D server for both the models (https://servicesn.mbi.ucla.edu/Verify3D/) [28].

2.4. Protein preparation and grid generation

Structures retrieved from protein data bank (https://www.rscb.org), were prepared using the inbuilt protein preparation module of Schrodinger. During the process of protein preparation, hydrogen atoms were added to the protein structure, further water molecules were removed with 3-angstrom distance from the nearby het groups. The structures were minimized and active sites of the proteins were predicted using the sitemap module for protein structures lacking co-crystallized ligand. However, the co-crystallized structure containing the bound ligand at the active site above step was skipped. Grid for molecular docking was generated either based on the predicted active site or using bound the co-crystallized ligand (Table 3). The internal grid size for docking purposes was 20 × 20 × 20 Å.

2.5. Molecular docking

The molecular docking approach is used for the identification and screening of potential lead molecules. The molecular docking studies

MolProbity Score	1.67
Clash Score	4.43
Ramachandran Favoured	93.10%
Ramachandran Outliners	0.0%

(A)

MolProbity Score	1.52
Clash Score	2.49
Ramachandran Favoured	91.85%
Ramachandran Outliners	2.58% A32 THR, A120 PRO, A45 LYS, A49 ASN, A114 PRO,

(B)

Figure 5. (A) Structure validation of Model 1 of TMPRSS2 using MolProbity (B) Structure validation of Model 2 of TMPRSS2 using MolProbity.

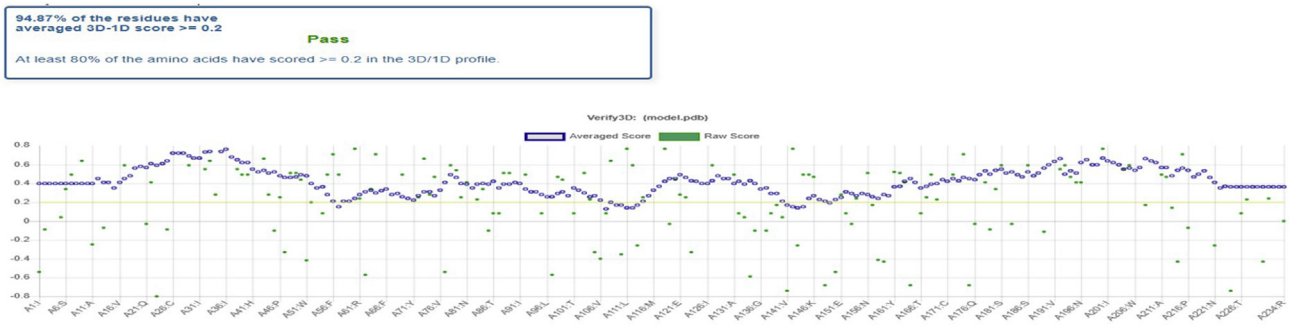

Figure 6. Structure Validation of Model 1 of TMPRSS2 using Verify3D.

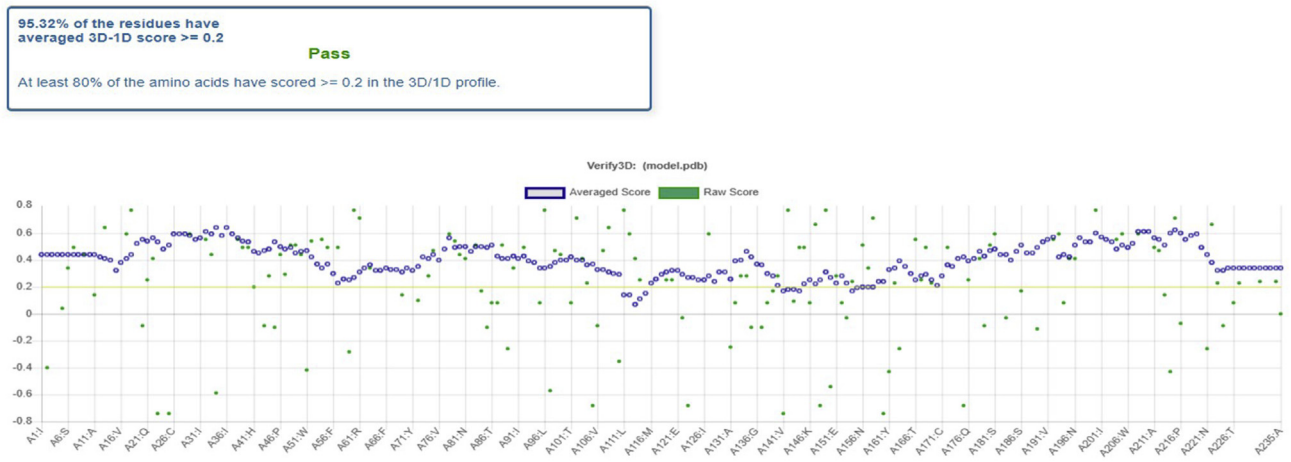

Figure 7. Structure Validation of Model 2 of TMPRSS2 using Verify3D.

provided us the information of key interacting residues between the protein of interest and generated ligands. It also helps in screening the large scale ligand data sets for drug development and repurposing. In this study SP protocol of Glide was used for molecular docking using the OPLS3e force field without making changes in the default parameter to predict the affinity of designed ligands against the multiple targets of the COVID-19. Ligand sampling was kept flexible. The ligand cut-off value for good binding interaction was selected as more than -5.5 kcal/mol, Any ligand with a score less than the mentioned score were considered to be having weak interaction. The efficient ligand against COVID-19 was selected using the following formula:

$$\text{Lig}_{\text{E Score}} = \sum \text{Dock Score (ACE2} + \text{NSP9} + \text{MPro} + \text{PL-Pro} + \text{SP} + \text{TMPRSS2)}$$

Validation of docking protocol was done through redocking of co-crystallized ligand present in M^{Pro} PDB file and superimposing the two crystal structures.

2.6. ADMET studies

ADMET studies play a crucial role in drug development, helping in the screening of ligands on their ADMET properties thus reducing the cost and time. 5 ligands with the highest Lig_E Score were shortlisted for the ADMET studies. The ADMET studies were executed using the ADMET LAB Server (http://admet.scbdd.com/home/index/).

3. Result and discussion

3.1. Homology modeling and structure validation

Two 3D structure models were built using Swiss-Model with GMQE score of 0.78 and 0.76, and QMEAN score of -0.67 and -2.46 respectively with a percentage identity of 42.92% and 44.87% suggesting the models developed are reliable and of good quality. The structure validation of the modelled protein structures was plotted graphically, the residues with a value below 0.6 were considered of poor quality. The two modelled structures also lied with the range of other protein structures hence confirming its reliability. The local quality estimate of the residues of predicted model 1 is given in Figure 4.

Ramachandran plot and its statistics for both the TMPRSS2 models were obtained using the MolProbity. Ramachandran plot statistics for model 1 implied that it has 93.10% of residues in the favored region and 0.0% in the outliner region with a clash score of 4.43 and MolProbity Score of 1.67. Similarly, Model 2 Ramachandran plot assessment implied 91.85% of residues are in the favored region, while residues A32 THR, A120 PRO, A46 PRO, A4 LYS, A49 ASN, and A114 PRO residues lied in the outliner region contributing to 2.58%. The clash score and MolProbity score for model 2 were 2.49 and 1.52 respectively (Figure 5).

Also, Verify3D of both modelled structures was obtained for the assessment and validation of structures and both the modelled showed result as PASS (Figures 6 and 7). Henceforth both developed models were validated.

3.2. Designed ligands and molecular docking analysis

In this study, a multiple target approach was utilized as it is desirable to consider such targets associated with infection or diseases [29, 30]. The molecular docking approach is also used for the prediction of targets against synthesized compounds, mi-rna or peptide based target inhibitors and also used for drug repurposing [30, 31, 32, 33]. We have designed annomontine based derivatives and performed molecular docking analysis against multiple targets of SARS-CoV-2 such as MPRO, ACE2, spike protein, etc. The study was designed to predict the ability of

Table 4. Molecular Docking results of annomontine based derivatives (ΔKcal/mol). (a)The Dock score is an average score of docked molecules of both Homology Generated TMPRSS Models. Note: The bold docking score represents the specific and Selective target for the compounds as compared to other targets.

Molecule	MPRO	ACE2	SP	NSP9	PLPRO	TMPRSS2[a]	LIG SUM
P3U	**-6.555**	-7.313	-4.201	-5.097	-4.572	-4.8345	-32.57
P3V	**-7.575**	-5.118	-3.947	-5.553	-4.041	-4.797	-31.03
P3A	-6.14	**-8.3**	-3.117	-5.556	-4.387	-3.31	-30.81
P3C	-5.879	**-6.338**	-4.723	-5.308	-3.749	-4.5285	-30.52
P3W	**-6.944**	-5.946	-3.237	-4.967	-4.623	-4.795	-30.51
P3E	-6.36	-7.187	-3.885	-4.629	-3.801	-4.215	-30.07
P3R	-5.878	-7.12	-3.197	-5.019	-4.232	-4.6255	-30.07
P3L	-6.028	-5.098	-4.037	-5.719	-4.165	-4.942	-29.98
P3I	-5.921	-3.999	-4.196	-5.448	-5.021	-5.2345	-29.81
P3B	-5.608	-6.49	-4.09	-5.138	-3.792	-4.465	-29.58
P3O	-5.818	-6.494	-3.66	-4.938	-4.055	-4.4965	-29.46
P1A	-6.331	-6.736	-2.841	-6.186	-2.794	-4.49	-29.37
P3K	-5.196	-5.754	-3.493	-5.364	-4.42	-4.892	-29.11
P3F	-6.055	-5.484	-4.381	-4.849	-3.899	-4.374	-29.04
P3M	-5.879	-4.924	-4.068	-5.545	-3.859	-4.702	-28.97
P3Q	-6.707	-6.003	-3.025	-4.582	-3.949	-4.2655	-28.53
P3D	-5.689	-6.345	-3.103	-4.934	-3.658	-4.296	-28.02
P3N	-5.51	-5.803	-3.568	-4.645	-3.699	-4.172	-27.39
P3J	-5.343	-5.334	-3.128	-5.102	-3.892	-4.497	-27.29
P3P	-5.676	-6.429	-3.185	-4.97	-3.01	-3.99	-27.26
P3G	-5.75	-5.457	-4.087	-4.4	-3.52	-3.96	-27.17
P3S	-4.949	-5.853	-3.08	-4.776	-3.803	-4.2895	-26.75
HCQ	-5.344	-5.733	-3.158	-4.276	-3.661	-4.45	-26.62
P3T	-5.44	-4.395	-2.507	-5.317	-3.938	-4.6275	-26.22
P3H	-5.569	-5.041	-2.302	-4.152	-3.431	-3.7915	-24.28

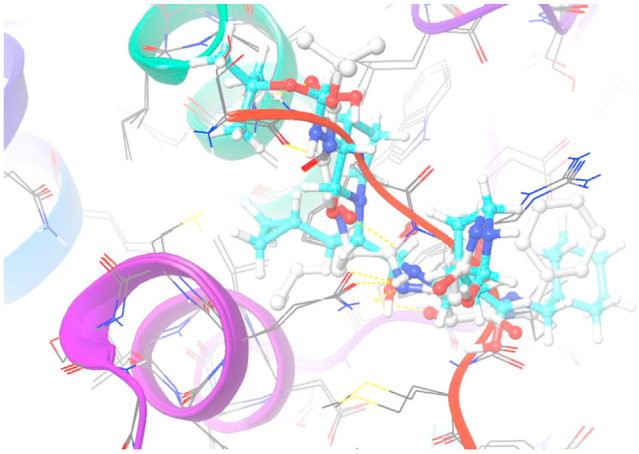

Figure 8. Validation of Docking protocol by redocking of crystal ligand and superimposition over the original crystal structure. The RMSD value of 2.0 Å.

annomontine derivatives binding to the targets, the efficiency of these derivates was computed by the summation of the docking Score against each target defined as $Lig_{E\ Score}$, based on the score predicted order of

Table 5. The molecular Docking Score of Known Inhibitors with their Target Protein.

PROTEIN	Inhibitor	Dock Score	Reference
Ace2	Hydroxychloroquine	-5.733	[34]
Mpro	GC-376	-7.4	[35]
Pl-Pro	Pl-Pro inhibitor	-4.0	[32, 36]
TMPRSS2	Cemostat	-4.53	[37]

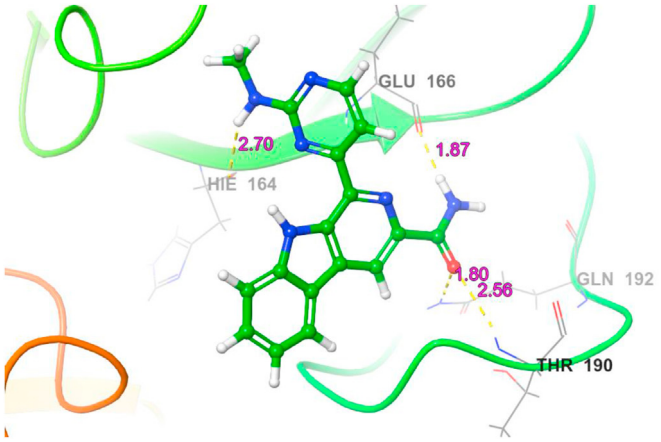

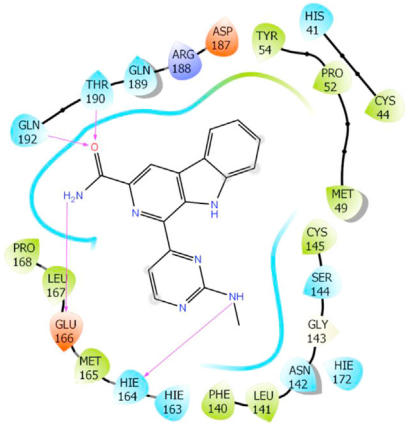

Figure 9. 3D and 2D interaction Diagram of M^{PRO} with P3V.

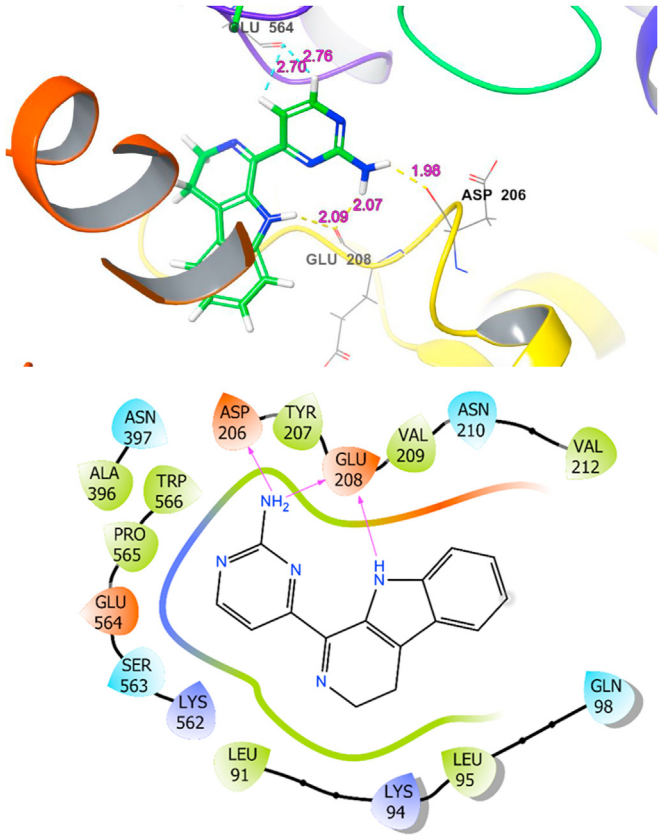

Figure 10. 2D and 3D interaction Diagram of ACE2 with P3A.

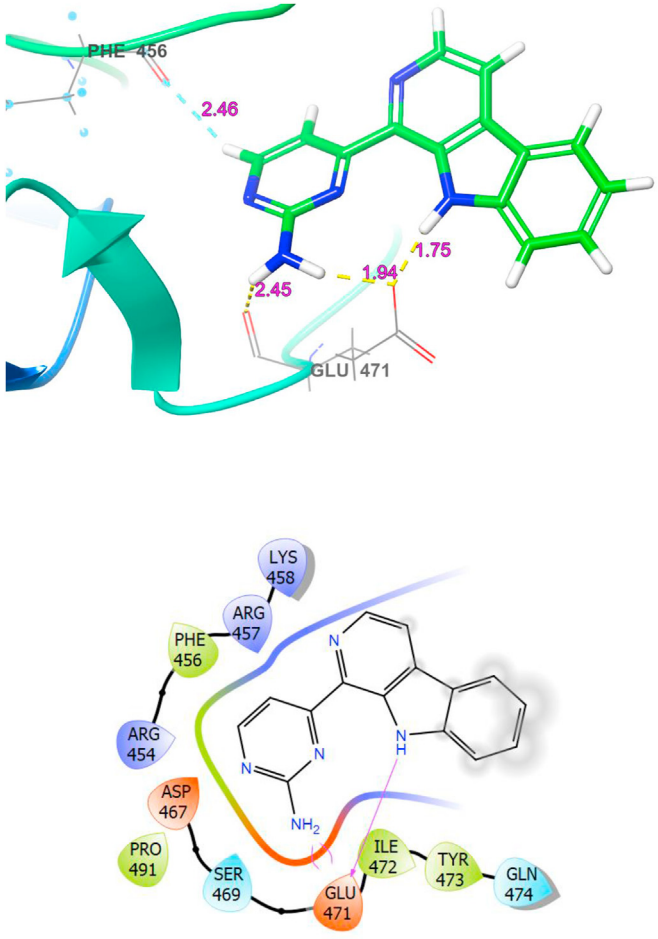

Figure 11. 2D and 3D interaction Diagram of Spike Protein with P3C.

docking efficiency for derivates was found to be **P3U** > **P3V** > **P3A** > **P3C** > **P3W** (Table 4).

To validate the docking protocol, redocking of co-crystallized ligand present in M^{Pro} PDB file and superimposing the two crystal structures. The calculated RMSD was found to be 2.0 Å (Figure 8). Also molecular docking analysis was performed against known inhibitors of target protein to act as a standard for reference (Table 5).

M^{PRO}, also known as 3CLPro plays a crucial role in viral replication, as it controls its activities of viral replication complex acting as the cysteine protease that helps in proteolytic cleavage of the precursor Polyproteins into functional proteins necessary for viral replication. M^{PRO} is composed of 3 structural domains, domain I consist of residues 8 to 101 while domain II consists of residues 102 to 184 residues having an anti-parallel β-sheet structure. Domain III consists of residues 201 to 303, structurally it consists of 5 α-helices organized into anti-parallel globular cluster connected to domain II with help of a loop region consisting of 15 residues from 185 to 200 [38]. The visualization of the co-crystallized ligand active site revealed the interaction of the ligand with HIS41, GLY143, CYS145, HIE163, HIE164, and GLU166 amino acid residues of the active site. The molecular docking analysis against M^{PRO} suggested increased molecular interaction of derivate **P3V** (Dock score -7.575), docking interaction diagram of **P3V** given in Figure 9 shows H-bond Interactions with GLU166 and GLN192. In this case $-NH_2$ of amide interacts with GLU166 and the carbonyl oxygen of the amide group shows H-bond interaction with GLN192 and THR190. Additionally, an H-bond was formed between Hydrogen of Amine and HIE164. However, increasing the length of H- Bond from 2.8Å to 3.5Å showed the formation of additional interactions with CYS145 that are also found in the co-crystallized ligand. Further emphasizing the potential of **P3V** as an M^{PRO} inhibitor.

ACE2, also known as Angiotensin-converting enzyme 2 interacts with the spike protein of SARS-Cov-2 and is considered to be the main Host receptor for its entry into cells [7]. It is expressed across various tissues in

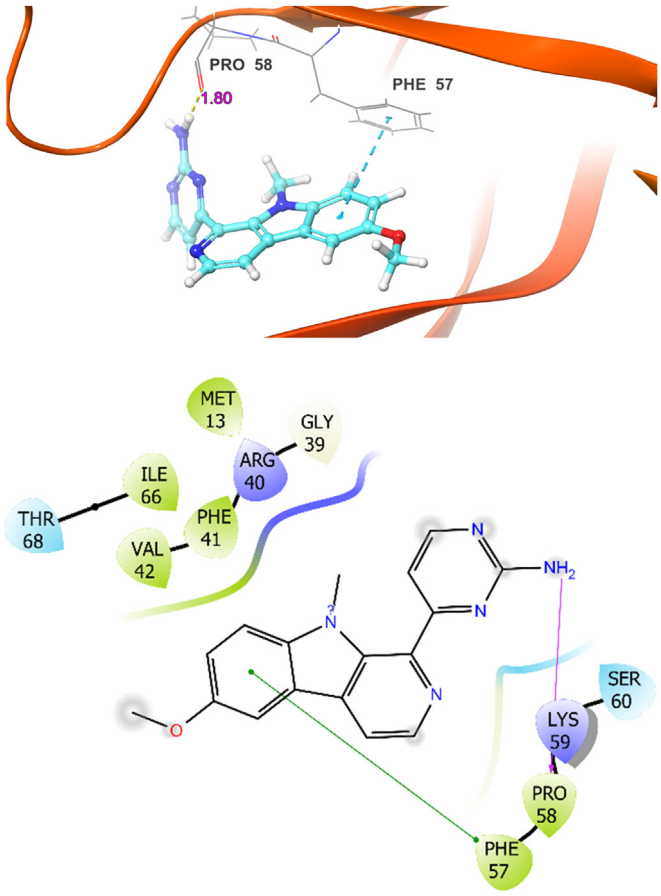

Figure 12. 2D and 3D interaction Diagram of NSP9 with P3L.

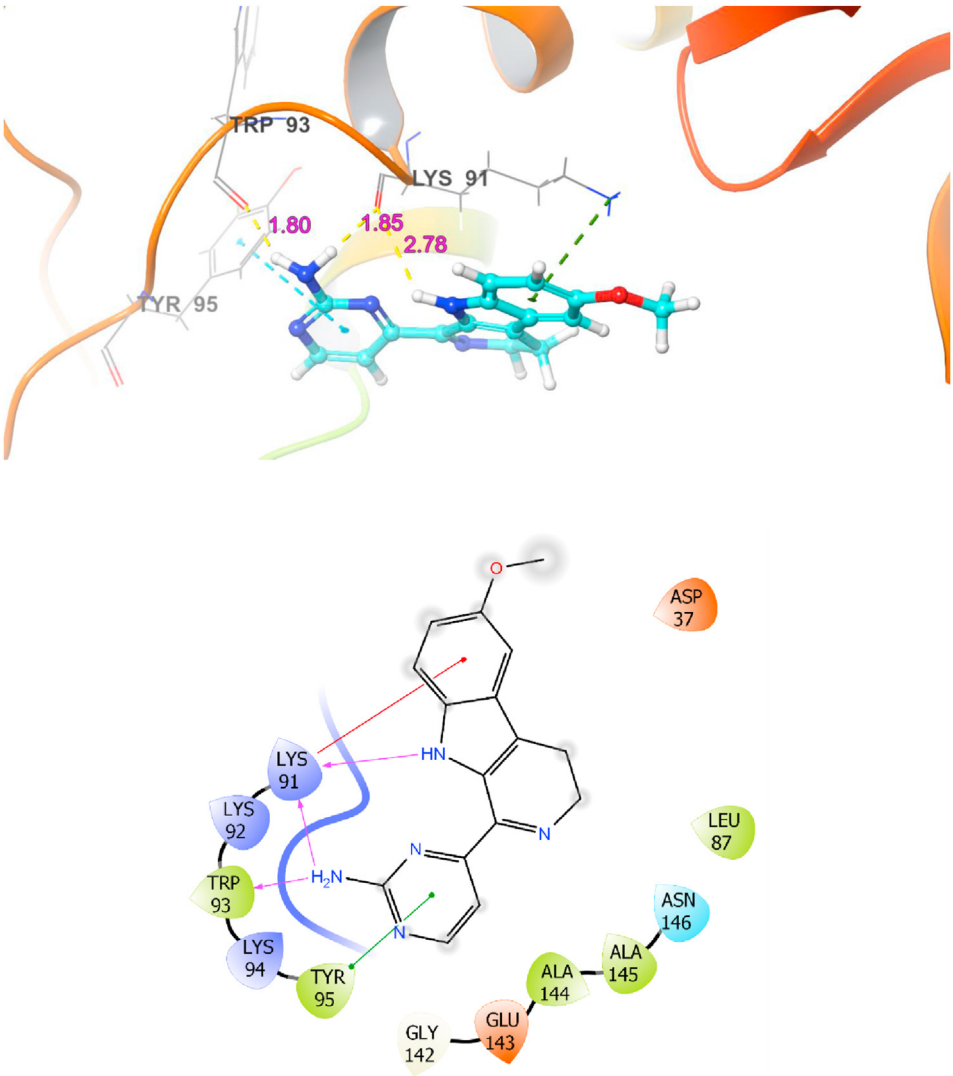

Figure 13. 2D and 3D interaction Diagram of PL^{Pro} with P3I.

the body, with a recent study reporting its high expression in mucosal tissue in the oral cavity [39]. Other tissues include lungs, kidney, etc [40]. The docking interaction of ACE2 with **P3A (**Dock Score -8.30) appeared to be more favorable compared to all others. The 3D and 2D interactions are shown in Figure 10 reveals H-bond interactions with GLU 208 and ASP206 (Figure 10). In this case, indole –NH and outer $–NH_2$ substituent of guanidine form H-bond interaction with the GLU208 in addition to the similar interaction of $–NH_2$ group of guanidine with ASP206. An additional two Aromatic H-bond were formed with Glu564. The Pi- Cat, and Pi-Pi interaction were completely missing in this case.

Instead, Spike Protein interacts with ACE2 which ensures the fusion of viral membrane and entry of viral load into the host cells. The spike protein docking analysis suggested **P3C** be a better derivative. However, the interaction score of -4.73 (Dock score), suggests comparatively weak binding of annomontine derivative against viral spike protein. The interaction diagram of **P3C** shown in Figure 11 shows H-bond interaction with GLU471, aromatic H-bond type interaction was found with PHE456. In this case outer $–NH_2$ group of guanidine forms two H-bonds and the indole –NH forms a single H-bond with GLU471 respectively. Based on molecular docking scores of annomontine derivates it can be concluded these derivates are not suitable for Spike Protein targeting and further structural modification should be considered in the existing famework.

NSP 9 is a non-structural protein considered to play a role in both viral replication and its virulence. Based on literature evidence, it is suggested that NSP 9 is indeed involved and plays a crucial role in the reproduction of the viral RNA genome, binding RNA *via* fold unique to the genre of β-coronavirus family, associated with alpha-helical GxxxG motif. The motif is considered to play an important role in coronavirus viral replication. However, the molecular mechanism is unclear at this stage. The disruption of this viral dimer interface is considered crucial for the prevention of its replication [41, 42]. The molecular docking results for NSP9 and annomontine derivatives suggested **P3L** best interacting derivate, interaction diagram revealed the formation of a single H- bond involving outer $–NH_2$ of guanidine and PRO58 residue of NSP9 protein (Figure 12). Similar to spike protein, annomontine derivatives bound weakly to the target and hence need further consideration in terms of structural modification to improve the overall binding affinity.

PL^{PRO} also referred to as Papain-Like protease, plays a role in the processing of three cleavage sites of SARS-CoV-2 viral polyproteins that result in the formation of nsp1, nsp2, and nsp3. It also possesses the deubiquitinase and deISGylating activity. Various attempts have been made to develop its inhibitor [43, 44, 45, 46, 47]. The annomontine docking with PLPRO suggested **P3I** as the best possible derivative with a docking score of -5.021 kcal/mol. However, the score is below the cut-off score of -5.50 kcal/mol and thus, the interaction can be considered weak. The interaction diagram revealed H- bond interaction between the $–NH_2$ of outer guanidine and LYS 91, TRP 93 (Figure 13). Furthermore, additional pi-cation interaction and pi-pi interaction was formed with LYS91

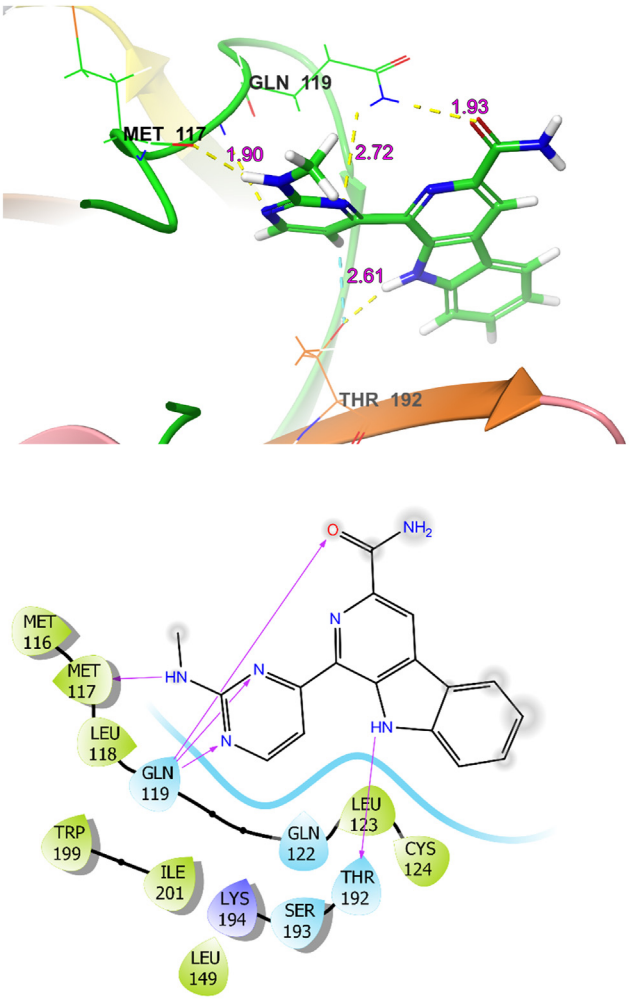

Figure 14. 2D and 3D interaction Diagram of TMPRSS2 with P3V.

and THR95 respectively. Similar to spike protein and NSP9, annomontine derivates bound weakly to the target and hence leaving the scope to fill up the void in terms of structural modification for enhances binding.

TMPRSS2 also referred to as transmembrane serine protease 2, is widely expressed across the epithelial cells of the lungs, gastrointestinal and urogenital tract of humans [48, 49]. Various studies have reported the role of TMPRSS2 as a virus activating protease and fusion activation [50, 51]. Inhibition of TMPRSS2 results in the inactivation of proteolytic activation of progeny virus thus inhibiting the spread of the virus [52, 53, 54, 55]. Activation of viral protein occurs at a monobasic cleavage site after TMPRSS2 cleaves at single arginine or lysine residue [56]. A recent study also indicated the role of TMPRSS2 in the activation of SARS-CoV-2 spike protein, [56, 57]. therefore, implying the potential of TMPRSS2 as a drug target for inhibition of viral infection from SARS-CoV-2. The molecular docking analysis was performed against the two generated homology models for TMPRSS2. The dock score for annomontine derivatives was taken as an average score against each model, the docking studies suggested **P3V** as the best annomontine derivate to target TMPRSS2 with average dock score of -6.38 kcal/mol. The molecular interaction diagram for model 1 revealed the formation of three H-Bonds with MET117, GLN119, and THR192 residues of TMPRSS2 (Figure 14). Additionally, aromatic H-bond interaction was formed with LEU123. In this case, outer –NH of guanidine forms H-bond with MET117, H-bond with O of amide forms H-bond with LYS194 and ring N of guanidine forms H-bond with GLN119. In contrast, the molecular interaction diagram for model 2 of TMPRSS2 revealed the formation of H-Bonds with GLN183, SER186, and GLY209. Additional aromatic H-bonds were formed with GLY209. In this case, outer –NH of guanidine forms H-bond with GLN183, O of amide forms H-bond with SER186, and indole –NH form H-bond with GLY209.

Further, post docking simulation ADME/TOX analysis was performed against the potential drug molecule for potetnt potentioa for COVID-19, the selection of potential drug like derivative was made using the $LigE_{Score}$. The top 5 derivatives with the highest $LigE_{Score}$ were selected and evaluated for the ADME/TOX analysis (Table 6), revealing that all the derivates have the potential of being hepatotoxic and induce damage to the liver. The derivatives **P3V** and **P3W** have the potential to be HERG blocker, however further validation and *in vitro* and *in vivo* studies are warranted for validation of efficiency and efficacy of annomontine derivative as a potential drug against COVID-19.

4. Conclusion

The study design is based on *in silico* approach that has successfully established a novel class of annomontine derivatives consisting of β-carboline architecture as potential lead molecules against SARS-CoV-2 targets. The global COVID pandemic has motivated the detailed computational analysis based on evaluation of docking scores rendered by the interaction of target proteins (M^{PRO}, PL^{PRO}, spike protein, ACE2, and TMPRSS2) with all the 23 ligands specifically designed for this purpose. The naturally present annomontine like methoxyannomontine, annomontine, and *N*-hydroxyannomontine were previously reported for having anti-malarial, anti-leishmanial activity, and anti-infective properties [26, 58]. These molecules were designed in accordance with the naturally occurring analogues like **P3K, P3L, P3M, P3N** are derivatives of methoxyannomontine while **P3O, P3P, P3Q, P3R, P3S, P3T** are derivatives of hydroxannomontine. Rest other 13 molecules are derivatives of annomontine. The derivatization of annomontine was done according to the synthesis, feasibility, and interaction ability. Amide and ester groups were known to exist in several drugs and have high reactivity because of the presence of hydrogen and oxygen that quickly bind with other molecules and form hydrogen bonds. The results validate our hypothesis as the derivatives having amide in their side chains show high interaction with different targets of SARS-CoV-2. Interestingly, the majority of these ligands displayed a better binding affinity with the target proteins as compared to the reference hydroxychloroquine which has been recently considered as an effective alternative in combination with azithromycin to combat COVID 19, and also compared to their known inhibitors while maintaining the similar binding interactions of those inhibitors. Among these 23 ligands, the binding studies of the top 5 novel annomontine analogs (**P3U > P3V > P3A > P3C > P3W)** against the multiple targets co-related to COVID-19 and its immunopathogenesis for their exceptional potentiality for further exploration in near future. Additionally, ADME/TOX study for these top 5 candidates against various biological descriptors ensured and supported their potential safety for biological administration. The outcome potentiates further *in-vitro* studies of the proposed annomontine derivatives and hence will be carried out to further validate the efficacy and efficiency of the novel annomontine derivatives against SARS-CoV-2.

Declarations

Author contribution statement

Kamran Waidha: Performed the experiments; Analyzed and interpreted the data; Contributed reagents, materials, analysis tools or data; Wrote the paper.

Anjali Saxena, Prashant Kumar: Performed the experiments; Wrote the paper.

Sunil Sharma: Conceived and designed the experiments.

Devalina Ray: Analyzed and interpreted the data; Contributed reagents, materials, analysis tools or data; Wrote the paper.

Table 6. ADME/TOX Prediction of Top 5 annomontine derivatives predicted using ADMETLAB.

	Molecule	P3U	P3V	P3A	P3C	P3W	Meaning and Preference
Physiochemical Properties	LogS (Solubility)	88.373 μg/ml	60.38 μg/mL	138.822 μg/mL	102.357 μg/mL	27.932 μg/mL	Optimal: higher than -4 log mol/L <10 μg/mL: Low solubility; 10–60 μg/mL: Moderate solubility; >60 μg/mL: High solubility
	$LogD_{7.4}$ (Distribution Coefficient D)	1.255	1.626	1.936	1.927	2.34	1 to 3: Solubility moderate: Permeability moderate; Metabolism low
	LogP (Distribution Coefficient P)	1.372	1.832	1.452	2.273	3.042	Optimal: 0 < LogP<3
Absorption	Papp (Caco-2 Permeability)	-5.344 cm/s	-5.224 cm/s	-4.854 cm/s	-4.7 cm/s	-5.458 cm/s	Optimal: higher than -5.15 Log unit or -4.70 or -4.80
	Pgp-inhibitor	Negative	Negative	Negative	Negative	Negative	
	Pgp-substrate	Negative	Negative	Positive	Positive	Negative	
	HIA (Human Intestinal Absorption)	0.84	0.84	0.75	0.86	0.793	≥30%: HIA+; <30%: HIA-
Distribution	PPB (Plasma Protein Binding)	74.58%	82.42%	70.45%	76.41%	94.35%	Significant with drugs that are highly protein-bound and have a low therapeutic index.
	VD (Volume Distribution)	-0.082 L/kg	0.044L/kg	0.577L/kg	0.406L/kg	-0.211 L/kg	Optimal: 0.04–20L/kg
	BBB (Blood–Brain Barrier)	0.885	0.59	0.89	0.93	0.722	
Metabolism	P450 CYP1A2 inhibitor	Positive	Positive	Positive	Positive	Positive	
	P450 CYP1A2 Substrate	Negative	Positive	Positive	Positive	Negative	
	P450 CYP3A4 inhibitor	Negative	Positive	Negative	Negative	Positive	
	P450 CYP3A4 substrate	Negative	Negative	Negative	Negative	Negative	
	P450 CYP2C9 inhibitor	Negative	Negative	Negative	Negative	Negative	
	P450 CYP2C9 substrate	Negative	Negative	Negative	Negative	Negative	
	P450 CYP2C19 inhibitor	Negative	Negative	Negative	Negative	Negative	
	P450 CYP2C19 substrate	Negative	Negative	Negative	Negative	Negative	
	P450 CYP2D6 inhibitor	Negative	Negative	Positive	Positive	Negative	
	P450 CYP2D6 substrate	Negative	Negative	Negative	Negative	Negative	
Elimination	$T_{1/2}$ (Half Life Time)	1.556 h	1.688 h	1.616 h	1.832 h	1.757 h	Range: >8h: high; 3h < Cl < 8h: moderate; <3h: low
	CL (Clearance Rate)	1.778 mL/min/kg	1.762 mL/min/kg	1.76 mL/min/kg	1.879 mL/min/kg	1.403 mL/min/kg	Range: >15 mL/min/kg: high; 5 mL/min/kg < Cl < 15 mL/min/kg: moderate; <5 mL/min/kg: low
Toxicity	hERG (hERG Blockers)	Negative	Positive	Negative	Negative	Positive	
	H-HT (Human Hepatotoxicity)	Positive	Positive	Positive	Positive	Positive	
	AMES (Ames Mutagenicity)	Negative	Negative	Negative	Positive	Negative	
	SkinSen (Skin sensitization)	Negative	Negative	Negative	Negative	Negative	
	LD50 (LD50 of acute toxicity)	1214.285 mg/kg	1025.395 mg/kg	638.936 mg/kg	634.044 mg/kg	910.14 mg/kg	High-toxicity: 1–50 mg/kg; Toxicity: 51–500 mg/kg; low-toxicity: 501–5000 mg/kg
	DILI (Drug Induced Liver Injury)	Positive	Positive	Positive	Positive	Positive	

Biswajit Saha: Conceived and designed the experiments; Analyzed and interpreted the data; Contributed reagents, materials, analysis tools or data; Wrote the paper.

Funding statement

Dr Biswajit Saha was supported by Science and Engineering Research Board (CS-192/2011) and Alexander von Humboldt-Stiftung.

Data availability statement

Data included in article/supplementary material/referenced in article.

Declaration of interests statement

The authors declare no conflict of interest.

Additional information

No additional information is available for this paper.

Acknowledgements

We are grateful to Amity University Uttar Pradesh for providing computational resources.

References

[1] B. S, M. Jk, L. Bn, W. Gr, Mechanisms of coronavirus cell entry mediated by the viral spike protein, Viruses 4 (2012). https://pubmed.ncbi.nlm.nih.gov/22816037/.
[2] L.-L. Ren, et al., Identification of a novel coronavirus causing severe pneumonia in human: a descriptive study, Chin. Med. J. (Engl.) 133 (2020) 1015–1024.
[3] C. Huang, et al., Clinical features of patients infected with 2019 novel coronavirus in Wuhan, China, Lancet Lond. Engl. 395 (2020) 497–506.
[4] W. Wang, J. Tang, F. Wei, Updated understanding of the outbreak of 2019 novel coronavirus (2019-nCoV) in Wuhan, China, J. Med. Virol. 92 (2020) 441–447.
[5] Q. Li, et al., Early transmission dynamics in Wuhan, China, of novel coronavirus-infected pneumonia, N. Engl. J. Med. 382 (2020) 1199–1207.
[6] W.G. Carlos, C.S. Dela Cruz, B. Cao, S. Pasnick, S. Jamil, Novel Wuhan (2019-nCoV) coronavirus, Am. J. Respir. Crit. Care Med. 201 (2020) P7–P8.
[7] R. Lu, et al., Genomic characterisation and epidemiology of 2019 novel coronavirus: implications for virus origins and receptor binding, Lancet Lond. Engl. 395 (2020) 565–574.
[8] A.R. Fehr, S. Perlman, Coronaviruses: an overview of their replication and pathogenesis, Methods Mol. Biol. Clifton NJ 1282 (2015) 1–23.
[9] R. McBride, M. van Zyl, B.C. Fielding, The coronavirus nucleocapsid is a multifunctional protein, Viruses 6 (2014) 2991–3018.
[10] F. Wu, et al., A new coronavirus associated with human respiratory disease in China, Nature 579 (2020) 265–269.
[11] E. de Wit, N. van Doremalen, D. Falzarano, V.J. Munster, SARS and MERS: recent insights into emerging coronaviruses, Nat. Rev. Microbiol. 14 (2016) 523–534.
[12] S. Perlman, J. Netland, Coronaviruses post-SARS: update on replication and pathogenesis, Nat. Rev. Microbiol. 7 (2009) 439–450.
[13] A. Zumla, J.F.W. Chan, E.I. Azhar, D.S.C. Hui, K.-Y. Yuen, Coronaviruses - drug discovery and therapeutic options, Nat. Rev. Drug Discov. 15 (2016) 327–347.
[14] D.E. Gordon, et al., A SARS-CoV-2 protein interaction map reveals targets for drug repurposing, Nature 583 (2020) 459–468.
[15] L. Caly, J.D. Druce, M.G. Catton, D.A. Jans, K.M. Wagstaff, The FDA-approved drug ivermectin inhibits the replication of SARS-CoV-2 in vitro, Antivir. Res. 178 (2020) 104787.
[16] P. Gautret, et al., Hydroxychloroquine and azithromycin as a treatment of COVID-19: results of an open-label non-randomized clinical trial, Int. J. Antimicrob. Agents 56 (2020) 105949.
[17] B. Saha, S. Sharma, D. Sawant, B. Kundu, Water as an efficient medium for the synthesis of tetrahydro-β-carbolines via Pictet–Spengler reactions, Tetrahedron Lett. 48 (2007) 1379–1383.
[18] B. Saha, R. Kumar, P.R. Maulik, B. Kundu, Synthesis of fused polycyclic nitrogen-containing heterocycles via cascade cyclization, Tetrahedron Lett. 47 (2006) 2765–2769.
[19] E.V. Costa, et al., A pyrimidine-beta-carboline and other alkaloids from Annona foetida with antileishmanial activity, J. Nat. Prod. 69 (2006) 292–294.
[20] N.H. Naik, A.K. Sikder, R.S. Kusurkar, Two new approaches towards the synthesis of annomontine using Pictet–Spengler and aza-Diels–Alder reactions, Tetrahedron Lett. 54 (2013) 3715–3717.
[21] C. Carmona, et al., Ground and singlet excited state hydrogen bonding interactions of betacarbolines, Phys. Chem. Chem. Phys. 2 (2000) 5076–5083.
[22] J.R.F. Allen, B.R. Holmstedt, The simple β-carboline alkaloids, Phytochemistry 19 (1980) 1573–1582.
[23] F. Arioglu, H. Altunbas, Harmane induces anxiolysis and antidepressant-like effects in rats, Ann. N. Y. Acad. Sci. 1009 (2003) 196–201.
[24] P. Hilber, P. Chapillon, Effects of harmaline on anxiety-related behavior in mice, Physiol. Behav. 86 (2005) 164–167.
[25] I. De-la-Cruz-Chacón, et al., Spatio-temporal variation of alkaloids in Annona purpurea and the associated influence on their antifungal activity, Chem. Biodivers. 16 (2019), e1800284.
[26] R.A. Costa, et al., Structural, vibrational, UV–vis, quantum-chemical properties, molecular docking and anti-cancer activity study of annomontine and N-hydroxyannomontine β-carboline alkaloids: a combined experimental and DFT approach, J. Mol. Struct. 1171 (2018) 682–695.
[27] A. Waterhouse, et al., SWISS-MODEL: homology modelling of protein structures and complexes, Nucleic Acids Res. 46 (2018) W296–W303.
[28] V.B. Chen, et al., MolProbity: all-atom structure validation for macromolecular crystallography, Acta Crystallogr. D Biol. Crystallogr. 66 (2010) 12–21.
[29] N.A. Murugan, S. Kumar, J. Jeyakanthan, V. Srivastava, Searching for target-specific and multi-targeting organics for Covid-19 in the Drugbank database with a double scoring approach, Sci. Rep. 10 (2020) 19125.
[30] S. Suresh, et al., Multi-component approach for synthesis of Quinolinyl-1,4-dihydropyridines, evaluation of cytotoxicity against MCF7 and molecular docking studies, ChemistrySelect 5 (2020) 10501–10510.
[31] S. Khurana, K. Waidha, R. Guleria, S. Sharda, S. Bose, In-silico investigations of selective miRNA-gene targets and their validation studies in obstructive sleep apnea (OSA) patient cohorts, Comput. Biol. Chem. 87 (2020) 107264.
[32] K. Ratia, et al., A noncovalent class of papain-like protease/deubiquitinase inhibitors blocks SARS virus replication, Proc. Natl. Acad. Sci. U. S. A. 105 (2008) 16119–16124.
[33] B. Shah, P. Modi, S.R. Sagar, In silico studies on therapeutic agents for COVID-19: drug repurposing approach, Life Sci. 252 (2020) 117652.
[34] N. Wang, et al., Chloroquine and hydroxychloroquine as ACE2 blockers to inhibit viropexis of 2019-nCoV Spike pseudotyped virus, Phytomedicine 79 (2020) 153333.
[35] M.D. Sacco, et al., Structure and inhibition of the SARS-CoV-2 main protease reveal strategy for developing dual inhibitors against Mpro and cathepsin L, Sci. Adv. 6 (2020) eabe0751.
[36] B.T. Freitas, et al., Characterization and noncovalent inhibition of the deubiquitinase and deISGylase activity of SARS-CoV-2 papain-like protease, ACS Infect. Dis. 6 (2020) 2099–2109.
[37] M. Hoffmann, et al., SARS-CoV-2 cell entry depends on ACE2 and TMPRSS2 and is blocked by a clinically proven protease inhibitor, Cell 181 (2020) 271–280, e8.
[38] Z. Jin, et al., Structure of M pro from SARS-CoV-2 and discovery of its inhibitors, Nature (2020) 1–5.
[39] H. Xu, et al., High expression of ACE2 receptor of 2019-nCoV on the epithelial cells of oral mucosa, Int. J. Oral Sci. 12 (2020) 1–5.
[40] I. Hamming, et al., Tissue distribution of ACE2 protein, the functional receptor for SARS coronavirus. A first step in understanding SARS pathogenesis, J. Pathol. 203 (2004) 631–637.
[41] D.R. Littler, B.S. Gully, R.N. Colson, J. Rossjohn, Crystal structure of the SARS-CoV-2 non-structural protein 9, Nsp9, iScience 23 (2020) 101258.
[42] Z.J. Miknis, et al., Severe acute respiratory syndrome coronavirus nsp9 dimerization is essential for efficient viral growth, J. Virol. 83 (2009) 3007–3018.
[43] R. Arya, A. Das, V. Prashar, M. Kumar, Potential Inhibitors against Papain-like Protease of Novel Coronavirus (SARS-CoV-2) from FDA Approved Drugs, 2020.
[44] Y.M. Báez-Santos, et al., X-ray structural and biological evaluation of a series of potent and highly selective inhibitors of human coronavirus papain-like proteases, J. Med. Chem. 57 (2014) 2393–2412.
[45] A.K. Ghosh, et al., Structure-based design, synthesis, and biological evaluation of a series of novel and reversible inhibitors for the severe acute respiratory syndrome-coronavirus papain-like protease, J. Med. Chem. 52 (2009) 5228–5240.
[46] A.K. Ghosh, et al., Severe acute respiratory syndrome coronavirus papain-like novel protease inhibitors: design, synthesis, protein-ligand X-ray structure and biological evaluation, J. Med. Chem. 53 (2010) 4968–4979.
[47] K. Ratia, et al., A noncovalent class of papain-like protease/deubiquitinase inhibitors blocks SARS virus replication, Proc. Natl. Acad. Sci. U. S. A. 105 (2008) 16119–16124.
[48] E. Böttcher-Friebertshäuser, Membrane-anchored serine proteases: host cell factors in proteolytic activation of viral glycoproteins, Act. Viruses Host Proteases (2018) 153–203.
[49] T.H. Bugge, T.M. Antalis, Q. Wu, Type II transmembrane serine proteases, J. Biol. Chem. 284 (2009) 23177–23181.
[50] E. Böttcher, et al., Proteolytic activation of influenza viruses by serine proteases TMPRSS2 and HAT from human airway epithelium, J. Virol. 80 (2006) 9896–9898.
[51] M. Hoffmann, H. Hofmann-Winkler, S. Pöhlmann, Priming time: how cellular proteases arm coronavirus spike proteins, Act. Viruses Host Proteases (2018) 71–98.
[52] B. Hatesuer, et al., Tmprss2 is essential for influenza H1N1 virus pathogenesis in mice, PLoS Pathog. 9 (2013).
[53] N. Iwata-Yoshikawa, et al., TMPRSS2 contributes to virus spread and immunopathology in the airways of murine models after coronavirus infection, J. Virol. 93 (2019).
[54] K. Sakai, et al., The host protease TMPRSS2 plays a major role in in vivo replication of emerging H7N9 and seasonal influenza viruses, J. Virol. 88 (2014) 5608–5616.
[55] C. Tarnow, et al., TMPRSS2 is a host factor that is essential for pneumotropism and pathogenicity of H7N9 influenza A virus in mice, J. Virol. 88 (2014) 4744–4751.
[56] D. Bestle, et al., TMPRSS2 and furin are both essential for proteolytic activation of SARS-CoV-2 in human airway cells, Life Sci. Alliance 3 (2020).
[57] M. Hoffmann, et al., SARS-CoV-2 cell entry depends on ACE2 and TMPRSS2 and is blocked by a clinically proven protease inhibitor, Cell 181 (2020) 271–280, e8.
[58] A.S. Nugraha, Y.D. Damayanti, P. Wangchuk, P.A. Keller, Anti-infective and anti-cancer properties of the Annona species: their ethnomedicinal uses, alkaloid diversity, and pharmacological activities, Mol. Basel Switz. 24 (2019).